JCB Journal of Cell Biology

REPORT

Cell size–dependent regulation of Wee1 localization by Cdr2 cortical nodes

Corey A.H. Allard, Hannah E. Opalko, Ko-Wei Liu, Uche Medoh, and James B. Moseley

Cell size control requires mechanisms that link cell growth with Cdk1 activity. In fission yeast, the protein kinase Cdr2 forms cortical nodes that include the Cdk1 inhibitor Wee1 along with the Wee1-inhibitory kinase Cdr1. We investigated how nodes inhibit Wee1 during cell growth. Biochemical fractionation revealed that Cdr2 nodes were megadalton structures enriched for activated Cdr2, which increases in level during interphase growth. In live-cell total internal reflection fluorescence microscopy videos, Cdr2 and Cdr1 remained constant at nodes over time, but Wee1 localized to nodes in short bursts. Recruitment of Wee1 to nodes required Cdr2 kinase activity and the noncatalytic N terminus of Wee1. Bursts of Wee1 localization to nodes increased 20-fold as cells doubled in size throughout G2. Size-dependent signaling was caused in part by the Cdr2 inhibitor Pom1, which suppressed Wee1 node bursts in small cells. Thus, increasing Cdr2 activity during cell growth promotes Wee1 localization to nodes, where inhibitory phosphorylation of Wee1 by Cdr1 and Cdr2 kinases promotes mitotic entry.

Introduction

Many cell types divide at a reproducible size because of poorly understood mechanisms that couple cell growth to cell cycle signaling (Dolznig et al., 2004; Ginzberg et al., 2015). In eukaryotes, the ubiquitous cyclin-dependent kinase Cdk1 triggers mitotic entry and cell division (Harashima et al., 2013). During G2, the protein kinase Wee1 phosphorylates and inhibits Cdk1 to prevent premature mitosis (Russell and Nurse, 1987; Gould and Nurse, 1989). The counteracting phosphatase Cdc25 removes this inhibitory phosphorylation to activate Cdk1 and promote mitotic entry (Russell and Nurse, 1986; Gautier et al., 1991; Kumagai and Dunphy, 1991; Strausfeld et al., 1991). The balance of Wee1 versus Cdc25 activity determines the timing of mitotic entry and cell division, meaning that cells require mechanisms to inhibit Wee1 and activate Cdc25 as they grow during G2 (Moreno et al., 1989).

This conserved Cdk1 activation system was initially identified and characterized in the fission yeast *Schizosaccharomyces pombe* (Russell and Nurse, 1986, 1987; Simanis and Nurse, 1986; Gould and Nurse, 1989). These rod-shaped cells grow by linear extension at the cell tips with no change in cell width and then enter mitosis and divide at a threshold size caused by the regulated activation of Cdk1 (Fantes and Nurse, 1977; Moreno et al., 1989). The concentration of Cdc25 protein increases as cells grow in G2, providing a simple mechanism for its size-dependent regulation (Moreno et al., 1990; Keifenheim et al., 2017). In contrast, the concentration of Wee1 protein remains constant during G2 (Aligue et al., 1997; Keifenheim et al., 2017), suggesting that size-dependent mechanisms altering Wee1 activity and/or localization might exist. A recent study identified progressive phosphorylation of Wee1 as cells grow during G2, raising the possibility that inhibitory kinases might increasingly act on Wee1 as cells grow (Lucena et al., 2017).

Genetic and biochemical studies have identified two SAD family protein kinases, Cdr1 and Cdr2, which act as upstream inhibitors of Wee1. Both deletion and kinase-dead mutations in *cdr1* and *cdr2* result in elongated cells caused by misregulation of Wee1 (Russell and Nurse, 1987; Young and Fantes, 1987; Wu and Russell, 1993; Breeding et al., 1998; Kanoh and Russell, 1998). Cdr1 can directly phosphorylate the Wee1 kinase domain to inhibit catalytic activity in vitro (Coleman et al., 1993; Parker et al., 1993; Wu and Russell, 1993). The role of Cdr2 kinase activity is less clear, but Cdr2 activation increases during cell growth in G2 (Deng et al., 2014). A key role for Cdr2 in this pathway is to assemble large, immobile node structures at the plasma membrane in the cell middle (Morrell et al., 2004). These interphase nodes are poorly defined oligomers of Cdr2, which then recruit Cdr1 to these sites (Martin and Berthelot-Grosjean, 2009; Moseley et al., 2009; Guzmán-Vendrell et al., 2015). Wee1 primarily localizes in the nucleus and the spindle pole body (SPB), where it can interact with Cdk1 (Wu et al., 1996; Moseley et al., 2009; Masuda et al., 2011). Wee1 has also been visualized at cortical nodes in some

Department of Biochemistry and Cell Biology, The Geisel School of Medicine at Dartmouth, Dartmouth, Hanover, NH.

Correspondence to James B. Moseley: james.b.moseley@dartmouth.edu.

https://doi.org/10.1083/jcb.201709171

studies (Moseley et al., 2009; Akamatsu et al., 2017) but not in others (Wu et al., 1996; Masuda et al., 2011), and the low expression level of endogenous Wee1 has prevented careful analysis of its potential association with nodes.

Two models have been suggested to explain the relay of cell size information to Wee1 through Cdr2 nodes. The first model depends on the Dual specificity tyrosine-phosphorylation–regulated kinase (DYRK) Pom1, which directly phosphorylates Cdr2 to inhibit kinase activation and mitotic entry (Martin and Berthelot-Grosjean, 2009; Moseley et al., 2009). Pom1 forms size-invariant concentration gradients that emanate from the cell tips and could act as cellular "rulers," but the concentration of Pom1 at the cell middle is largely independent of cell size, and *pom1Δ* mutants retain size homeostasis (Hachet et al., 2011; Saunders et al., 2012; Wood and Nurse, 2013; Bhatia et al., 2014; Pan et al., 2014). An alternative model suggests that the accumulation of Cdr2 nodes, which double in number as cells double in size, generates size-dependent control of Wee1 (Pan et al., 2014). A limitation of previous studies has been the inability to monitor the signaling "output" of nodes because it has been unclear if, how, and when endogenous Wee1 localizes to nodes. Additionally, it has been unknown how nodes and their constituent proteins influence Wee1 phosphorylation in vivo.

In this study, we found that nodes are stable megadalton-sized complexes required for proper Wee1 phosphorylation in cells. By live-cell total internal reflection fluorescence (TIRF) microscopy, we discovered that endogenous Wee1 localizes to Cdr2 nodes in transient bursts. The frequency and duration of bursts scale with cell size, and Pom1 regulates this node output specifically in small cells. Our combined results support a model whereby Cdr2 activity increases as cells grow, leading to size-dependent inhibition of Wee1 at nodes. This size-dependent pathway likely combines with other sizing mechanisms including Cdc25 accumulation to generate the homeostatic cell size control system.

Results and discussion

Nodes are stable complexes that promote Wee1 phosphorylation

Cells require mechanisms to turn off Wee1 as they grow during G2 and approach the threshold size for division. Recent work identified progressive phosphorylation of Wee1 during this growth phase by monitoring a shift in Wee1 migration by SDS-PAGE (Lucena et al., 2017). Genetic studies place Cdr1 and Cdr2 kinases as upstream inhibitors of Wee1, but direct evidence of Wee1 phosphoregulation by Cdr1 and Cdr2 kinases in cells has been lacking. By monitoring the phosphorylation-dependent shift of endogenous Wee1 migration in Western blots, we found that the most highly phosphorylated forms of Wee1 were absent in *cdr1Δ* mutants (Fig. 1 A). This result supports previous in vitro evidence for direct phosphorylation of Wee1 by Cdr1 (Coleman et al., 1993; Parker et al., 1993; Wu and Russell, 1993). Wee1 collapsed to a single band in *cdr2Δ* cells (Fig. 1 A), indicating a more dramatic loss of Wee1 phosphorylation in this mutant. These results show that Cdr1 and Cdr2 regulate phosphorylation of Wee1 in cells and point to a key role for Cdr2 in this process. Cdr2 assembles into stationary nodes at the plasma membrane during G2 and recruits Cdr1 to these sites (Morrell et al., 2004; Martin and Berthelot-Grosjean, 2009; Moseley et al., 2009; Guzmán-Vendrell et al., 2015). To test whether assembly of Cdr2 and Cdr1 into nodes is important for Wee1 phosphorylation in cells, we blotted against Wee1 in *cdr2ΔC* cells. This mutant lacks the C-terminal KA1 domain that binds to both lipids and Cdr1, but it retains the Cdr2 kinase and ubiquitin-associated domains that are required for catalytic activity. As a result, Cdr2ΔC does not bind the cortex or form nodes, and instead it localizes diffusely to the cytoplasm and nucleus (Fig. 1 B; Moravcevic et al., 2010; Deng et al., 2014; Guzmán-Vendrell et al., 2015). We observed loss of Wee1 phosphorylation in the *cdr2ΔC* mutant similar to a *cdr2Δ* mutant (Fig. 1 C). We conclude that node-based signaling by Cdr1 and Cdr2 regulates phosphorylation of Wee1 in cells.

The biophysical nature of Cdr2 nodes has been unclear. For example, these structures could represent stable biochemical complexes, or alternatively, they could be comprised of weakly aggregated proteins. The critical role of nodes in Wee1 signaling led us to investigate their stability in cell lysates. Using TIRF microscopy, we observed node-like structures in the lysates of *cdr2-monomeric EGFP* (*mEGFP*) cells (Fig. 1 D). These structures were absent in the lysates of *cdr2ΔC-mEGFP* cells and in lysates of control cells that do not express GFP (Fig. 1 D). This result suggests that nodes remain intact upon cell lysis and may represent stable complexes. To test this possibility, we performed subcellular fractionation of detergent extracts on velocity sucrose gradients. The mutant *cdr2ΔC* was found in early fractions representing monomeric proteins and/or small complexes (Fig. 1 E). In contrast, full-length Cdr2 migrated in a broad pattern with a peak at 60S (Figs. 1 E and S1, A and B), consistent with a megadalton-sized complex. These fractions could be dialyzed and centrifuged on a second sucrose gradient without altering the sedimentation pattern of Cdr2 (Fig. S1 C), suggesting that nodes contain a stable core. TIRF microscopy of sucrose gradient fractions from Cdr2-mEGFP cells revealed node-like structures in later fractions and diffuse signal in earlier fractions (Fig. S1 D). Thus, Cdr2 nodes represent large stable complexes as revealed by independent imaging and biochemical approaches.

Cdr2 is activated by phosphorylation of threonine 166 (T166) by the kinase Ssp1, and levels of Cdr2-pT166 increase with cell size (Deng et al., 2014). To determine the distribution of activated Cdr2 within our sucrose gradients, we used a phosphospecific antibody that detects Cdr2-pT166. We found that Cdr2-pT166 was enriched in the larger "node" fractions and largely absent from the smaller fractions (Fig. 1 E). This suggests that nodes are sites for concentration of activated Cdr2. Large node fractions contain very low levels of Cdr1 (Fig. S1 E), suggesting that it might not stably associate with the core of nodes. Consistent with this possibility, FRAP experiments revealed rapid turnover of Cdr1-mEGFP molecules at nodes in vivo (Fig. S1 F). We were unable to detect Wee1 in sucrose gradient experiments because of its low levels of expression and stability in lysates. These combined experiments identify a stable core of activated Cdr2 that forms cortical node structures for regulation of Wee1.

A second set of nodes assembled by the protein Blt1 associate with Cdr2 nodes late in the cell cycle (Moseley et al., 2009;

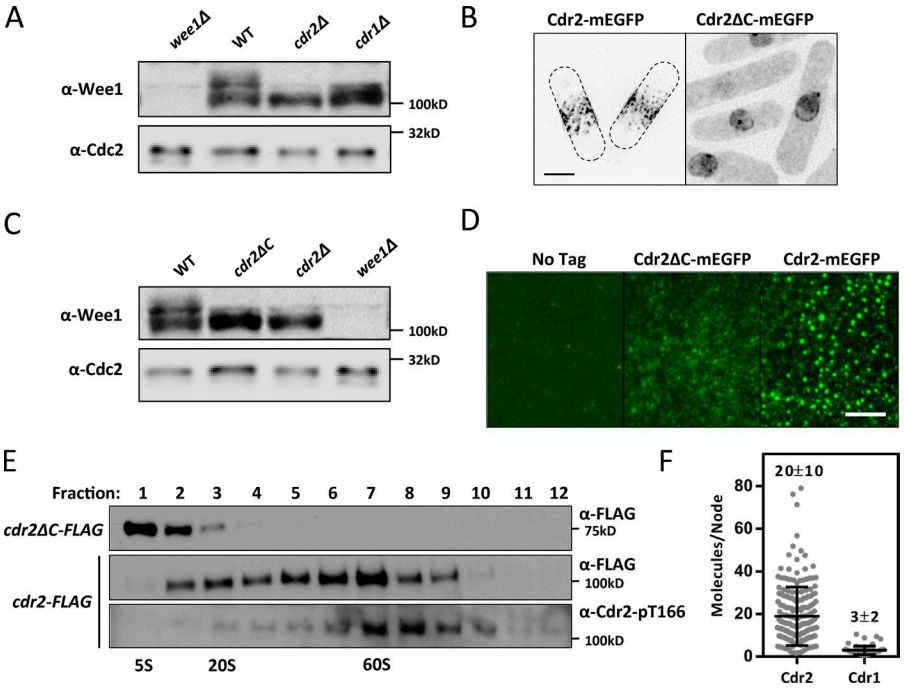

Figure 1. **Nodes are stable scaffolds that facilitate inhibition of Wee1. (A)** Wee1 phosphorylation is disrupted in *cdr1Δ* and *cdr2Δ* cells. Whole-cell extracts were separated by SDS-PAGE, and endogenous Wee1 was detected by Western blotting. **(B)** Localization of Cdr2-mEGFP and Cdr2ΔC-mEGFP in cells. Maximum-intensity projections from z series are shown. **(C)** Wee1 phosphorylation is disrupted in *cdr2ΔC* cells. Whole-cell extracts were analyzed as in A. Data in A and C are taken from the same Western blot, and the *wee1Δ* lane is the same in both. **(D)** Visualization of node-like puncta by TIRF microscopy in whole-cell extracts from the indicated strains. Bars, 5 µm. **(E)** Detergent extracts from *cdr2-FLAG* or *cdr2ΔC-FLAG* cells were subjected to velocity sucrose gradient sedimentation, and fractions were probed against the FLAG tag or against Cdr2(pT166). Fraction 1 corresponds with the top of the gradient and contains smaller complexes; fraction 12 corresponds with bottom of the gradient. S values were determined using size standards run on identical gradients. **(F)** Quantification of the number of Cdr2 and Cdr1 molecules per node (means ± SD; $n > 65$ each) based on superresolution live-cell fluorescence microscopy.

Akamatsu et al., 2014). Velocity sucrose gradients revealed the presence of Blt1 in a large protein complex in both WT and *cdr2Δ* cells (Fig. S1 I). Similarly, Cdr2 still sedimented in node fractions in *blt1Δ* cells, which lack this second set of node structures (Fig. S1 I). This result is consistent with previous microscopy studies showing Cdr2 nodes in *blt1Δ* cells and Blt1 nodes in *cdr2Δ* cells (Moseley et al., 2009; Akamatsu et al., 2014). Thus, Cdr2 forms a ∼60S node complex independently of Blt1 nodes.

For comparison with our biochemical fractionation, we used quantitative superresolution fluorescence microscopy to estimate the size of nodes in live cells. Using known measurements from previous research (Wu and Pollard, 2005), we calibrated a confocal microscope to measure fluorescence intensity per mEGFP molecule (Fig. S1, G and H). With this setup, we imaged *cdr2-mEGFP* and *cdr1-mEGFP* cells and then calculated both global and local molecule numbers. The low expression level of Wee1-mEGFP prevented reliable in vivo molecule counting. Each cell contained a mean of 5,600 ± 1,000 Cdr2-mEGFP molecules as well as 700 ± 200 Cdr1-mEGFP molecules. More importantly, we used Airyscan confocal microscopy to measure 20 ± 10 molecules of Cdr2 per node as well as 3 ± 2 molecules of Cdr1 per node (Fig. 1 F), similar to independent studies using different imaging systems (Pan et al., 2014; Akamatsu et al., 2017). A node containing 20 Cdr2 molecules would be nearly 2 MD in size, and a globular complex of this size would sediment at ∼60S, consistent with our sucrose gradient fractionation (Fig. S1 B). We note that both in vitro and in vivo approaches independently revealed a large spread in the size of nodes, which suggests that nodes can assume a range of sizes that could relate to their signaling properties. Overall, we conclude that nodes are large stable structures organized by an oligomeric core of Cdr2 molecules. These structures and their components are required for phosphorylation of Wee1 in cells.

Wee1 localization to nodes requires Cdr2 kinase activity and the Wee1 N terminus

To begin investigating how Wee1 is regulated by nodes, we tested its physical association with Cdr2. In a yeast two-hybrid assay, Wee1 was previously shown to interact with the Cdr2 kinase domain, and this interaction was lost in the catalytically inactive *cdr2(E177A)* mutant (Guzmán-Vendrell et al., 2015). We confirmed this interaction and then used it to determine the domain of Wee1 critical for Cdr2 interaction and for localization to nodes. The Wee1 protein is comprised of a C-terminal protein kinase domain and an N-terminal region of unknown function (Fig. 2 A). The N-terminal 150 residues of Wee1 were both necessary and sufficient to interact with Cdr2 in yeast two-hybrid experiments, and these interactions were abolished by Cdr2(E177A) mutations (Fig. 2 B). This result is consistent with association of the Wee1 N terminus with Cdr2 in cell lysates (Kanoh and Russell, 1998) and suggests the possibility that the Wee1 N terminus functions to regulate localization to nodes. To test this idea, we examined localization of different Wee1 constructs after overexpression. Full-length Wee1 localized to nodes, but Wee1(151–end), a truncated mutant lacking the Cdr2 association domain, did not localize to nodes (Fig. 2 C). Thus, the Wee1 N terminus associates with Cdr2 and is required for localization to Cdr2 nodes. Although Wee1(1–150) was sufficient to interact with Cdr2 in the yeast two-hybrid assay, it was not sufficient for node localization in cells (Fig. 2 C), meaning that additional residues or structural features of Wee1 might contribute to its ability to localize to nodes upon overexpression.

Next, we tested the functional role of the Wee1 N terminus by integrating a truncation mutant expressed by the endogenous promoter as the sole copy of Wee1 in the cell. *wee1(151–end)* cells were elongated at division (Fig. 2 D), consistent with loss of Wee1 inhibition by the node pathway. This phenotype was not additive

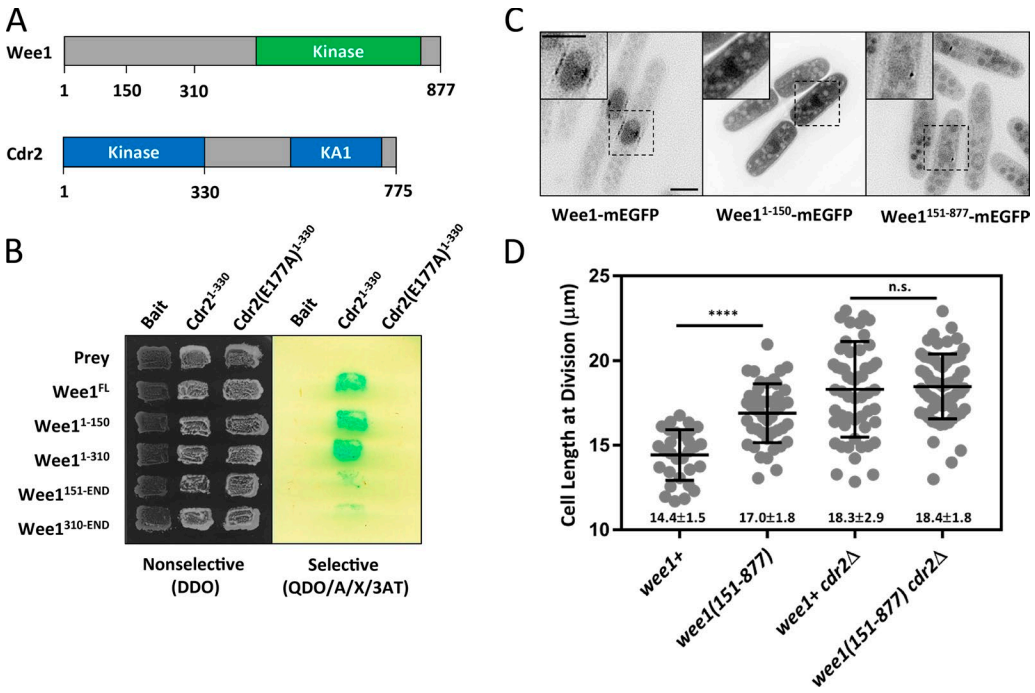

Figure 2. **Wee1 localization to nodes requires Cdr2 kinase activity and the Wee1 N terminus. (A)** Schematic of Wee1 and Cdr2 functional domains. Values represent amino acid positions. **(B)** The Wee1 N terminus interacts with WT Cdr2 but not with kinase-dead Cdr2(E177A) in the yeast two-hybrid assay. Transformants were selected on a double-dropout (DDO) plate, and interactions were tested on a quadruple-dropout plate containing aureobasidin, X-gal, and 3-AT (QDO/A/X/3AT) plate. Positive interactions are indicated by growth of blue colonies on selective plates. **(C)** Localization of the indicated Wee1 constructs overexpressed from the P81nmt1 promoter. Middle–focal plane widefield images with inverted contrast are shown, and insets show enlarged views of dashed boxes. Bars, 5 µm. **(D)** Length of dividing septated cells of the indicated genotypes (means ± SD; $n > 50$ cells). ****, $P < 0.0001$; n.s., $P > 0.05$.

with *cdr2Δ*, suggesting that the Wee1 N terminus is required for regulation by Cdr2 (Fig. 2 D). In contrast, integrated full-length *wee1⁺* controls had no defects in cell size at division. These experiments show that the Wee1 N terminus is required for interaction with Cdr2, localization to nodes, and negative regulation of Wee1 function.

Dynamic bursts of Wee1 localization to Cdr2 nodes

Overexpressed Wee1 exhibits strong localization to Cdr2 nodes (Moseley et al., 2009), but localization of endogenously expressed Wee1 to nodes has been unclear. Wee1 is found in the nucleus and SPB, where it can associate with its inhibitory target Cdk1 (Wu et al., 1996; Moseley et al., 2009; Masuda et al., 2011). Our results implicate nodes as sites of Wee1 regulation by Cdr2 and Cdr1, suggesting that endogenous Wee1 might localize to nodes. However, because of its low expression levels, there have been conflicting data as to whether endogenous Wee1 localizes to cortical puncta (Moseley et al., 2009; Akamatsu et al., 2017) or does not localize to the cell cortex (Masuda et al., 2011). When seen at the cortex, low levels of Wee1 have prevented colocalization and time-lapse analyses. To study endogenous Wee1 at the cell cortex, we used the bright and photostable fluorophore mNeonGreen in combination with TIRF microscopy. In TIRF, we observed unambiguous Wee1-mNeonGreen localization at cortical puncta (Fig. 3 A). Strikingly, time-lapse imaging revealed that Wee1-mNeonGreen localized transiently to the cortex. From videos and kymographs, we found that Wee1 puncta bound and released the cell cortex with variable dwell times ranging from one frame (200 ms) to >1 min (Fig. 3 A and Video 1). Thus, endogenous Wee1 localizes to cortical nodes in transient bursts.

The transient nature of Wee1 localization to cortical nodes in TIRF contrasts with the other node proteins Cdr1 and Cdr2, which appear static in time-lapse videos from epifluorescence and confocal imaging systems. We performed four sets of experiments to support the conclusion that Wee1 transiently associates with stable Cdr2-Cdr1 nodes. First, we imaged endogenously tagged Cdr2-mNeonGreen or Cdr1-mNeonGreen in the same TIRF system. Both Cdr2-mNeonGreen and Cdr1-mNeonGreen persisted over long timescales at cortical nodes (Fig. 3 B and Videos 2 and 3), meaning that transient bursts are a specific behavior of Wee1 at nodes and are not an artifact of TIRF imaging. Second, we imaged Wee1 with a different fluorophore (Wee1-mEGFP) and observed transient bursts similar to Wee1-mNeonGreen. Third, we tested whether the position of the fluorophore at the Wee1 C terminus induced transient bursts. We generated an N-terminal tag (mEGFP-Wee1) and an in-frame internal tag (Wee1-mEGFPint) integrated at the endogenous locus and expressed under control of the endogenous *wee1* promoter. These constructs also exhibited transient localization bursts to cortical nodes (Fig. S2, A and B). Fourth, using two-color TIRF, we found that Wee1-mNeonGreen bursts colocalized with Cdr2-mRuby2 nodes (Fig. 3 C) but not with other cortical structures like eisosomes or Skb1-Slf1 nodes (Fig. S2, D and E). These combined experiments confirm that Wee1 localizes to Cdr2-Cdr1 cortical nodes in transient bursts, in contrast with other node components.

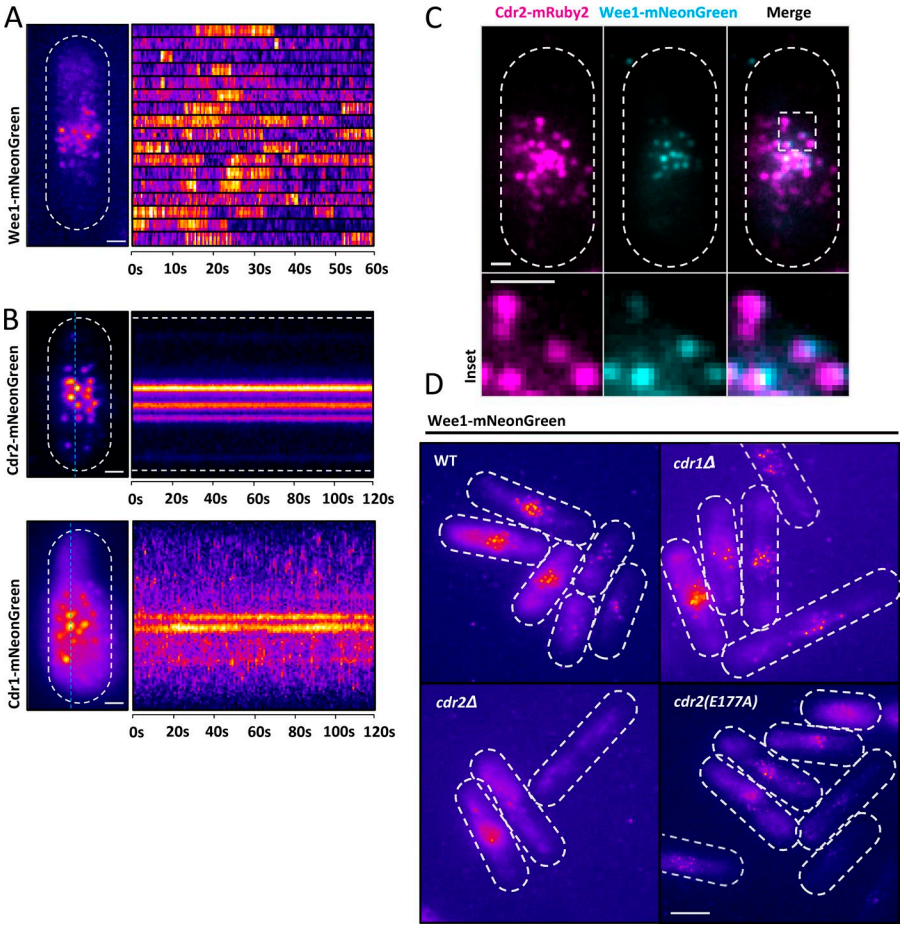

Figure 3. **Wee1 puncta bind transiently to stable Cdr2 nodes. (A)** Localization of Wee1-mNeonGreen by TIRF microscopy. Left: Maximum-intensity projection of a 60-s time series imaged at 1-s intervals. Right: Single-node 3 × 3–pixel kymographs of each Wee1 burst that appeared during the 60-s time lapse. See Video 1. **(B)** Cdr2 and Cdr1 are stationary during 2-min TIRF microscopy time-lapse acquisitions. Left: Maximum-intensity projections of time-lapse acquisitions with 1-s intervals. Right: Kymographs of the time lapse along the cyan dashed line. See Videos 2 and 3. **(C)** Wee1 bursts colocalize with Cdr2 nodes. Images are dual-channel simultaneously acquired TIRF microscopy images. **(D)** Localization of Wee1 by TIRF microscopy in the indicated strains. Images are maximum-intensity projections of 60-s time lapses imaged at 1-s intervals. Bars: (A–C) 1 µm; (D) 5 µm.

We next examined the molecular requirements for Wee1 node bursts. Wee1 puncta were unaffected in *cdr1Δ* cells but were absent from *cdr2Δ* cells (Fig. 3 D), which lack cortical nodes. Wee1 puncta were also reduced in the kinase-dead *cdr2(E177A)* mutant (Figs. 3 D and S2 I). We confirmed that these Wee1 bursts were at Cdr2(E177A) nodes using two-color TIRF microscopy on *wee1-mNeonGreen cdr2(E177A)-mKate2 cells* (Fig. S2 C). Cdr2(E177A)-mEGFP still forms cortical nodes and still recruits Cdr1 to nodes (Morrell et al., 2004; Moseley et al., 2009). Furthermore, Cdr2(E177A)-mEGFP nodes appeared identical to WT by superresolution molecule counting and FRAP experiments (Fig. S2, F and G). These results suggest that bursts of Wee1 localization to inhibitory nodes might serve as a functional output for Cdr2-based kinase signaling. Furthermore, regulation of Cdr2 kinase activity has the potential for dynamic control of Wee1 through node bursts.

The frequency of Wee1 node bursts increases with cell size

Wee1 is progressively phosphorylated as cells increase in size during G2 phase (Lucena et al., 2017), and we have shown that phosphorylation requires the inhibitory kinases Cdr1 and Cdr2. If Wee1 localization bursts to Cdr2 nodes mediate this progressive inhibitory phosphorylation, then we would predict size-dependent changes in Wee1 node bursts. Consistent with this prediction, Wee1 localization at nodes increased dramatically with cell size (Fig. 4 A). To quantify this increase, we measured the number of Wee1-mNeonGreen puncta visible in TIRF microscopy images taken with a 1-s exposure as a function of cell length. This analysis revealed a progressive increase in the number of Wee1 nodes as a function of cell size, resulting in a 20-fold difference in Wee1 nodes in large cells versus small cells (Fig. 4 B). Because many small cells lack detectable Wee1 nodes and TIRF imaging is restricted to a single plane, this 20-fold increase may underestimate the increase over the entire cell surface.

Both the frequency and duration of Wee1 bursts might be modulated to generate this cell size dependency. The number of Cdr2 nodes doubles during growth in G2 (Deng and Moseley, 2013; Pan et al., 2014; Akamatsu et al., 2017), which we corroborated by measuring the number of Cdr2-mEGFP nodes in the TIRF field as a function of cell size (Fig. S3 A). This twofold increase in Cdr2 node number likely contributes to the 20-fold increase in Wee1 localization at nodes by increasing the frequency of total bursts within a cell. However, the difference in scale indicates that additional regulatory mechanisms must exist. Therefore, we asked whether the duration of Wee1 bursts changes as a function of cell size. Time-lapse TIRF microscopy of Wee1-mNeonGreen revealed that the mean dwell time of Wee1 bursts is significantly correlated with cell size (slope of linear regression significantly nonzero; **, P = 0.002). Wee1 bursts in smaller cells lasted 6 ± 6 s (mean ± SD; *n* = 4 cells in size range 7–9 µm), and this duration doubled to ∼14 ± 17 s in large cells (mean ± SD; *n* = 4 cells in size range 14–16 µm; Fig. 4 C). Size-dependent accumulation of Wee1

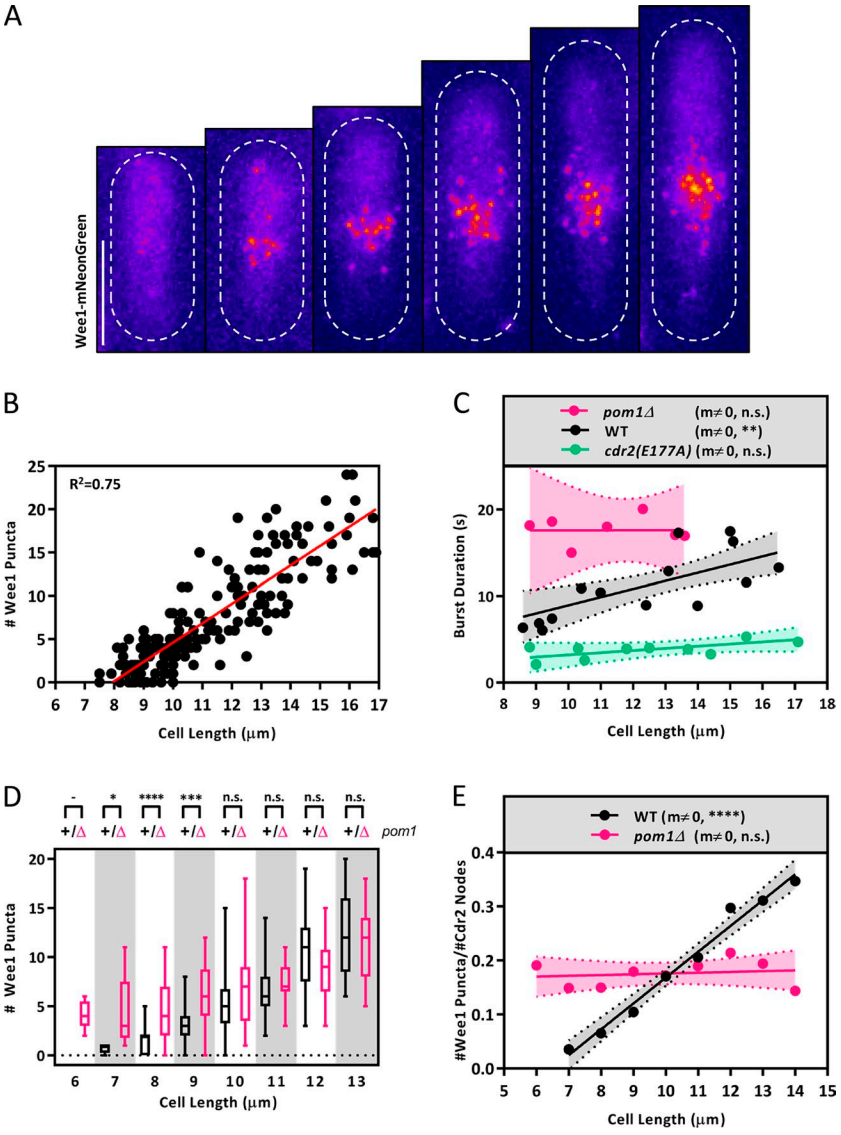

Figure 4. **Wee1 accumulation at nodes is size dependent and buffered by Pom1. (A)** Representative images of Wee1 node localization in cells of increasing size imaged by TIRF microscopy. Bar, 5 µm. **(B)** Quantification of the number of Wee1 puncta as a function of cell size. Values were obtained from TIRF images with 1-s exposure. Data fit a linear regression model. **(C)** Wee1 burst duration scales with cell size in WT but not *cdr2(E177A)* or *pom1Δ* cells. The duration of individual Wee1-mNeonGreen bursts was measured using time-lapse TIRF microscopy for cells of the indicated genotype. Dots correspond with mean burst duration plotted as a function of cell size. Lines are linear regressions fit to these data. Dotted lines indicate the 95% confidence interval of the linear regression accounting for SD and sample size of the mean for each data point. The resulting slope is significantly nonzero (m ≠ 0) for WT (P = 0.002; R^2 = 0.02) but not for *pom1Δ* (P = 0.01; R^2 = 0.01) or *cdr2(E177A)* (P = 0.9; R^2 = 3.3e^{-7}). **(D)** Pom1 suppresses Wee1 bursts in small cells. The number of Wee1 puncta was quantified as in B for WT and *pom1Δ* cells, and the data were binned according to cell size. Boxes indicate means and SD, and whiskers indicate minimum and maximum values. The number of Wee1 bursts is significantly different between WT and *pom1Δ* in the three smallest bins (7 µm: *, P = 0.01; 8 µm: ****, P < 0.0001; 9 µm: ***, P = 0.0003; 10–13 µm: P > 0.5). The 6-µm bin contains only *pom1Δ* cells ($n_{bin(WT/pom1Δ)}$) = 6 µm (0/5), 7 µm (4/10), 8 µm (28/23), 9 µm (34/24), 10 µm (32/25), 11 µm (17/21), 12 µm (21/15), and 13 µm (21/21). **(E)** Relative accumulation of Wee1 puncta and Cdr2 nodes in WT and *pom1Δ* cells as a function of cell size. Linear regressions and 95% confidence intervals are shown. The slope of the linear regression is significantly nonzero for WT (P < 0.0001; R^2 = 0.98) but not for *pom1Δ* (P = 0.7; R^2 = 0.26).

nodes was unaffected in *cdr1Δ* or *blt1Δ* cells but was strongly reduced in kinase-dead *cdr2(E177A)* mutant cells (Fig. S2, H–K). Cdr2 kinase activity was also required for size-dependent change in Wee1 burst duration. In *cdr2(E177A)* mutant cells, Wee1 bursts lasted ∼3.8 s regardless of cell size (n = 10; Fig. 4 C). This result indicates that Cdr2 kinase activity detains Wee1 at a node. We conclude that increases in Cdr2 kinase activity and node number contribute to size-dependent regulation of Wee1 bursts.

Pom1 suppresses Wee1 node bursts in small cells

We next tested how Pom1-Cdr2 signaling impacts size-dependent bursts of Wee1 to nodes. Pom1 directly phosphorylates Cdr2 to inhibit mitotic entry through Wee1. This modification inhibits node assembly and prevents the activating kinase Ssp1 from phosphorylating the Cdr2 activation loop (Moseley et al., 2009; Bhatia et al., 2014; Deng et al., 2014; Rincon et al., 2014; Guzmán-Vendrell et al., 2015; Kettenbach et al., 2015). The levels of activated Cdr2 increase as cells grow, raising the possibility that Pom1 might inhibit Cdr2 activation and downstream signaling events in a size-dependent manner (Deng et al., 2014). In *pom1Δ* cells, the size dependence of Wee1 node accumulation was partially disrupted because of increased Wee1 localization at nodes in small cells (Fig. 4 D). Wee1 puncta in large cells were unaffected by lack of Pom1. Because Pom1 inhibits Cdr2 kinase activity, which regulates the duration of Wee1 bursts, we wondered whether Pom1 acts in part by affecting the duration of Wee1 bursts. In *pom1Δ* cells, Wee1 burst duration was uniformly high (∼17.7s) and was independent of cell size (n = 7; Fig. 4 C). We conclude that Pom1 functions to reduce the duration of Wee1 bursts to inhibitory Cdr2 nodes in small cells. This activity likely contributes to premature mitotic entry in *pom1* mutant cells, whereas additional mechanisms maintain size-dependent regulation of Wee1 localization in larger cells.

Our data suggest that Pom1-dependent control of Cdr2 acts in combination with the twofold increase in Cdr2 node number, and these two combined factors generate the 20-fold increase in Wee1 localization to nodes. To test this possibility, we measured how Wee1 node bursts scale with Cdr2 node number in WT versus *pom1Δ* cells. In WT cells, the number of Wee1 puncta scales more steeply with cell size than the number of Cdr2 nodes, suggesting

Cdr2 node number alone does not explain the frequency of Wee1 bursting. In contrast, in *pom1Δ* cells, the ratio of Wee1 node bursts to Cdr2 node number was constant across a range of cell sizes (Fig. 4 E). Thus, in the absence of Pom1 regulation, the number of Wee1 node bursts scales with the number of Cdr2 nodes: both double as cell size doubles. Pom1 acts within this context to inhibit Cdr2 kinase activity and thereby suppress Wee1 node bursts in small cells. The effect of this Pom1 activity is to magnify the fold increase in Wee1 inhibition as cells double in size. These combined mechanisms contribute to the ∼20-fold increase in Wee1 bursts to inhibitory nodes as cells double in size.

Our work presents a framework to understanding the signaling steps that occur within a Cdr2 cortical node (Fig. 5). We found that Cdr2 kinase activity regulates Wee1 localization to nodes as previous work demonstrated that Cdr1 inhibits Wee1 kinase activity through phosphorylation (Coleman et al., 1993; Parker et al., 1993; Wu and Russell, 1993). These distinct regulatory mechanisms act on different domains of the Wee1 protein. Cdr2 phosphorylates the N-terminal domain that we found is critical for node localization (Kanoh and Russell, 1998), whereas Cdr1 phosphorylates the C-terminal kinase domain of Wee1 (Coleman et al., 1993; Parker et al., 1993; Wu and Russell, 1993). These results raise the possibility that initial phosphorylation by Cdr2 traps Wee1 molecules at a node for several seconds, allowing subsequent phosphorylation by Cdr1, which results in a catalytically inactive Wee1 molecule. Such processive phosphorylation would be consistent with partial loss of Wee1 phosphorylation in *cdr1Δ* cells, with more severe loss of phosphorylation in *cdr2Δ* cells. Future work will be directed at mapping residues phosphorylated by Cdr1 versus Cdr2 and elucidating the ultrastructural organization of these molecules within megadalton-sized nodes. We also note that nodes represent sites of Wee1 inhibition, whereas the nucleus and SPB are sites of Wee1 overlap with Cdk1. These two pools likely exchange through nuclear shuttling, which presents another potential point of regulation as cells grow and progressively inhibit Wee1. As cells grow, the increased frequency of Wee1 bursts to inhibitory nodes likely decreases cellular Wee1 activity, thus contributing to Cdk1 activation for mitotic entry.

Our data support a model whereby Wee1 regulation by the Cdr2–Cdr1 pathway is cell size dependent because of the combination of Pom1 activity in small cells and Cdr2 node accumulation. Mutations in this pathway alter cell size at division but do not impair cell size homeostasis (Wood and Nurse, 2013). This is not surprising given the existence of other size-dependent signaling mechanisms such as accumulation of the mitotic inducer Cdc25 (Moreno et al., 1990; Keifenheim et al., 2017), which also may not be solely responsible for cell size homeostasis. We consider it likely that cell size homeostasis is a robust systems-level property that emerges from the integration of multiple size-dependent signaling pathways including the node-based mechanism studied in our research. In this sense, it will be interesting to uncover how these different mechanisms connect, converge, and alter each other's signaling properties. Finally, cell size is modulated by nutrient availability in fission yeast and other organisms. The *cdr2* and *cdr1* mutants were initially identified because of altered cell cycle regulation upon nitrogen stress (Young and Fantes, 1987; Feilotter et al., 1991), and the Pom1–Cdr2

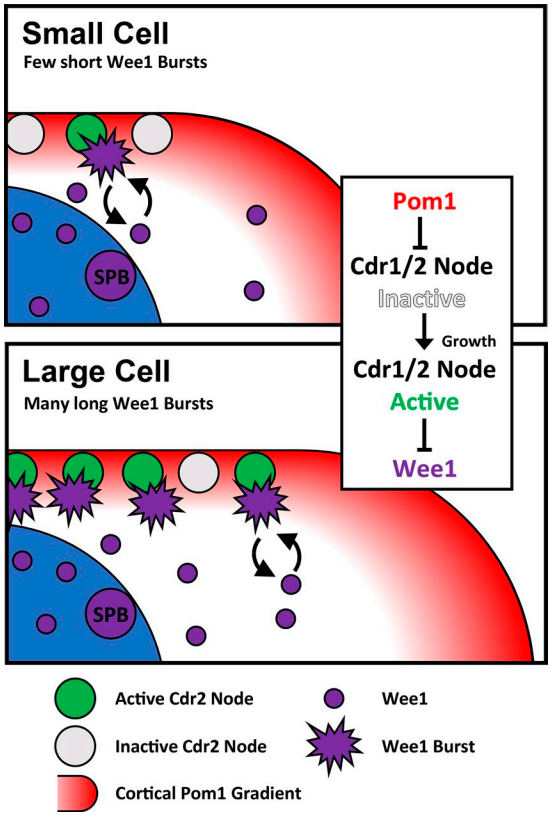

Figure 5. **A working model for size-dependent control of Wee1 by bursts of node localization.** See text for discussion.

pathway was recently implicated in cell cycle control during glucose deprivation (Kelkar and Martin, 2015). How environmental signals control Wee1 node bursts or other aspects of node-based signaling may reveal new mechanisms within this network.

Materials and methods

Strain construction and media

Standard *S. pombe* media and methods were used (Moreno et al., 1991). Strains used in this study are listed in Table S1. For cell length measurements, >50 septated cells from log-phase cultures grown in Edinburgh minimal medium + supplement (EMM4S) at 25°C were measured by Blankophor staining. Gene tagging and deletion were performed using PCR and homologous recombination (Bähler et al., 1998). Truncation of the endogenous Wee1 N terminus was performed by first deleting aa 1–150 from plasmid pJK148-Pwee1-wee1-Twee1 (pJM426) using QuikChange II mutagenesis (Agilent Technologies) to yield pJK148-Pwee1-wee1(151–877)-Twee1 (pJM1374). The parental and mutated plasmids were linearized by NruI digestion, integrated into the leu1 locus of strain JM777 (*wee1Δ::ura4 ura4-D18 leu1-32*), and selected on Edinburgh minimal medium–Leu plates. The mNeonGreen sequence was used under license from Allele Biotechnology. We concluded that this tag did not impair Wee1 function because *wee1-mNeonGreen* cells divided at 14.6 ± 1.1 µm in length (means ± SD for $n > 50$ cells grown in EMM4S at 32°C).

Sucrose gradient ultracentrifugation

Fission yeast detergent extracts were prepared by growing 1.5 liters of cells to mid-log phase (OD ∼0.3) and washing 2× with 50 ml node isolation buffer (NIB; 50 mM Hepes, 100 mM KCl, 1 mM $MgCl_2$, and 1 mM EDTA, pH 7.5). The pellet was then resuspended in an equal volume of 2× NIB (wt/vol) containing a protease/phosphatase inhibitor cocktail (10 µl/ml 200× protease inhibitor, 50 µl/ml of 1 M β-glycerol phosphate, 50 µl/ml of 1 M NaF, 2.5 µl/ml of 200 mM PMSF, and 1 µl/ml of 1 M DTT) and snap frozen as pellets by pipetting into a liquid nitrogen bath. Yeast pellets were then ground using liquid nitrogen–chilled coffee grinders for 2 min and then collected into chilled falcon tubes and stored at −80°C. 1.5 g of frozen yeast powder was then thawed on ice, Triton X-100 was added to a final concentration of 1%, and the extracts were mixed by gentle pipetting. Extracts were then centrifuged at 4°C for 10 min at 20,000 *g* to yield a low-speed supernatant, which was then subjected to sucrose gradient fractionation.

Discontinuous sucrose gradients were prepared by layering 5–23% (top to bottom) sucrose in NIB + 1% Triton X-100 in 1.2-ml steps of 2% sucrose increments. 400 µl low-speed detergent-extracted supernatant was then added to the top of the gradient. Sucrose gradients were centrifuged at 100,000 *g* (35,000 rpm) in a Beckman Coulter L8-M ultracentrifuge for 3.5 h at 4°C in a chilled SW41 swinging bucket rotor. 1 ml gradient fractions were collected from the top by hand and vortexed, and then 100 µl of each fraction was mixed 2:1 in 3× Western blot sample buffer (65 mM Tris, pH 6.8, 3% SDS, 10% glycerol, 10% 2-mercaptoethanol, 50 mM NaF, 50 mM β-glycerophosphate, and 1 mM sodium orthovanadate) and boiled for 5 min. Samples were then subjected to SDS-PAGE and Western blotting. Size standards were centrifuged and fractionated on individual gradients as described above and then subjected to SDS-PAGE and Coomassie staining (BSA and thyroglobulin) or by spectrophotometry (Ferritin). Stained gels were digitized, and band intensities were quantified using ImageJ (National Institutes of Health). The fraction corresponding with the sedimentation peak was used to calculate the sedimentation coefficient of Cdr2 in Fig. S2 B.

Western blotting

For gel-shift Western blots, whole-cell extracts were lysed in 100 µl of 3× Western blot sample buffer in a Mini-beadbeater-16 (Biospec) for 2 min. Gels were run at a constant 20 mAmps until a 75-kD marker was at the bottom of the gel. Blots were probed with mouse anti-FLAG M2 (Sigma-Aldrich) and rabbit anti-Wee1 (Deng and Moseley, 2013). For Wee1 Western blots, we also repeated each experiment with a different rabbit anti-Wee1 antibody (provided by D.R. Kellogg; Lucena et al., 2017), which yielded identical results (not depicted). For monitoring Wee1 phosphorylation, samples were run on an SDS-PAGE gel containing 6% acrylamide and 0.02% bisacrylamide.

For sucrose-gradient Western blots, samples were prepared as described above and run at a constant voltage of 100 mV on 10% acrylamide gels. Blots were probed with mouse anti–FLAG M2, rabbit anti–Cdr2-pT166 (Deng et al., 2014), or mouse anti-HA (clone 16B12; BioLegend). To reduce background signal, nitrocellulose membranes for phosphospecific Western blots were incubated in 4% BSA/TBS–Tween-20 for both primary and secondary antibodies at 4°C with 2-h washes in between.

Yeast two hybrid

A Matchmaker yeast two-hybrid system (Takara Bio Inc.) was used to test for physical interactions between Cdr2 and Wee1 constructs. Bait plasmids were generated by ligating PCR-amplified fragments into pGBKT7 using XmaI–SalI restriction sites. Prey plasmids were generated by ligating PCR fragments into pGADT7 using NdeI–XmaI restriction sites. All bait and prey plasmids were transformed into budding yeast strain Y2H-gold on single dropout plates (Synthetic defined–Leu or -Trp) and tested individually for autoactivation of the reporters on quadruple dropout plates (Synthetic defined–Leu-Trp-Ade-His) with X-gal, 125 ng/ml aureobasidin, and 30 mM 3-amino-1,2,4-triazole (QDO/X-/A/3AT). The full-length Cdr2 bait construct induced autoactivation, and so we used a truncated construct containing Cdr2 AA1-330 to test pairwise interactions. For interaction tests, bait and prey plasmids were cotransformed into Y2H-gold cells and selected on double-dropout plates (Synthetic defined–Trp-Leu) before scoring of interactions on QDO/X/A/3AT plates.

Widefield microscopy and analysis

Cells in Fig. 1 B were imaged in liquid EMM4S at 25°C using a DeltaVision imaging system (Applied Precision Ltd.) composed of an IX-71 inverted widefield microscope (Olympus) with a 100× UPlan Apochromat 1.40 NA oil objective, a CoolSnap HQ2 camera (Photometrics), and an Insight solid-state illumination unit (Applied Precision Ltd.). Z stacks were acquired at 0.5-µm intervals and processed by iterative deconvolution using SoftWoRx software (Applied Precision Ltd.). 2D maximum-intensity projections of these z stacks were rendered using ImageJ.

TIRF microscopy and analysis

Node components were imaged using simultaneous dual-color TIRF microscopy to limit excitation of fluorophores to those nearest to coverslip. Imaging was performed on a commercially available TIRF microscope (Micro Video Instruments) equipped with a 100× Apochromat TIRF 1.49 NA objective (Nikon) and a two-camera imaging adapter (Tu-CAM; Andor Technology) containing a dichroic and polarization filters (FF580-FDi01-25 × 36, FF02-525/40-25, and FF01-640/40-25; Semrock) to split red and green signal between two aligned iXon electron-multiplying charge-coupled device cameras (Andor Technology) using Elements software (Nikon). Red/green beam alignment was performed before imaging using a TetraSpeck fluorescent microsphere size kit (Thermo Fisher Scientific).

Standard #1.5 glass coverslips were RCA cleaned before use to remove fluorescent debris. Cells were grown in EMM4S and washed into fresh EMM4S immediately before imaging to remove autofluorescent puncta resulting from overnight culture. Cells were imaged in EMM4S media on glass slides at 25°C. Individual slides were used for ≤5 min to prevent cells from exhausting nutrients or oxygen. Agar pads were not used because of increased background fluorescence.

Image analysis and processing was performed using ImageJ. Cdr2 node numbers, Wee1 puncta numbers, and binding duration

were quantified using the MosaicSuite ParticleTracker plugin (Sbalzarini and Koumoutsakos, 2005). Because of variable fluorescence intensity in different TIRF fields and images, thresholding parameters were determined separately for each image, and accuracy was confirmed by visual inspection to ensure that only nodes/puncta were counted and that no nodes/puncta were omitted. Particle diameter was set to 1 pixel. Linking range for particle tracking was set to 2 pixels because neither Cdr2 nodes nor Wee1 puncta exhibited appreciable cortical diffusion on the time scale of our imaging. Lookup table was adjusted to fire for images in Figs. 3, 4, and S2 to emphasize signal intensities. Statistical significance of differences in Wee1 burst accumulation (Fig. 4 D) was determined using a Welch's *t* test.

Single-molecule counting

Local and cellular molecule counting were performed as by Wu and Pollard (2005). To determine the number of Cdr1 or Cdr2 molecules per node, we calibrated a fluorescence microscope to determine the local number of mEGFP molecules based on fluorescence intensity. A standard curve relating fluorescence intensity to the number of molecules per structure was created by imaging mEGFP-tagged Cdc12, Spn1, or Sad1, which have known numbers of molecules at their respective structures. These strains were provided by J.-Q. Wu (The Ohio State University, Columbus, OH). We then imaged Cdr2-mEGFP or Cdr1-mEGFP in the same genetic background. Cells were grown in YE4S to mid-log phase, concentrated, and imaged on YE4S agar pads at 25°C using identical imaging parameters. To achieve maximum resolution and sensitivity, imaging was performed on a commercially available LSM880 laser scanning confocal microscope (ZEISS) equipped with a 100× Plan Apochromat 1.46 NA oil objective, an Airyscan superresolution module and GaAsP detectors, and Zen Blue acquisition software (ZEISS) using the resolution versus sensitivity mode to optimize signal to noise. For each strain, we collected 40-slice z stacks with 0.17-µm spacing to image completely through entire cells with high spatial resolution in all dimensions. Airyscan images were processed in Zen Blue software, and quantification was performed on sum projections of Airyscan-reconstructed stacks. For preparation of the standard curve, integrated fluorescence density of Cdc12-mEGFP at cytokinesis nodes or contractile rings, Sad1-mEGFP at SPBs, and Spn1-mEGFP at septin rings was measured, and background signal was subtracted using an equal-sized region of interest (ROI) in ImageJ. Fluorescence values were then plotted against their known molecular counts to generate the standard curve. Fluorescence intensity of Cdr2-mEGFP or Cdr1-mEGFP at single-node ROIs was measured using identical imaging conditions and analysis, and their fluorescence values were plotted against the best-fit line of the standard curve to infer the number of molecules per node.

For determination of the cellular concentrations of Cdr1 and Cdr2, we similarly calibrated a Quorum Wave FX-X1 spinning-disk confocal system (Quorum Technologies) equipped with an ImageEM camera (Hamamatsu Photonics), a 100× Plan Apochromat VC 1.40 NA oil objective, and MetaMorph acquisition software (Molecular Devices). A standard curve relating fluorescence intensity to cellular concentration was created by imaging mEGFP-tagged Cdc12, Spn1, Sad1, Ain1, Rlc1, or Mid1, which have known cellular concentrations. These strains were provided by J.-Q Wu. We then imaged Cdr2-mEGFP or Cdr1-mEGFP in the same genetic background. Cells were grown in YE4S to mid-log phase, concentrated, and imaged on YE4S agar pads at 25°C using identical imaging parameters. We collected a z stack comprised of 13 slices with 0.5-µm spacing with the shutter open between steps. Sum projections were created from the entire stack, corrected for uneven illumination, and processed to remove background fluorescence and autofluorescence. Fluorescence intensity was measured from whole-cell ROIs using ImageJ. Fluorescence values were then plotted against their known molecular counts to generate the standard curve. Fluorescence intensities of Cdr2-mEGFP or Cdr1-mEGFP cells were measured using identical imaging conditions and analysis, and their fluorescence values were plotted against the best-fit line of the standard curve to infer the number of molecules per cell.

FRAP

FRAP analysis was performed using an LSM880 microscope (see the Single-molecule counting section) using the resolution versus sensitivity mode to decrease photobleaching during time lapses and to optimize signal to noise. Cells were grown in YE4S to mid-log phase, concentrated, and imaged on YE4S agar pads at 25°C. At each time interval, three optical-section z stacks with 0.16 µm spacing for 0.48 µm total thickness were acquired, processed with linear 2D Airyscan reconstruction, and used to generate sum-projection images of each time point for quantification using ImageJ. Bleaching was performed using Zen Black FRAP software (ZEISS) to bleach ROIs drawn around the node-containing region on one side of the cell. Unbleached cells were used to correct for photobleaching of the sample during acquisition. Data were fit to one-phase association curves from which the mobile fraction and $t_{1/2}$ were calculated.

Online supplemental material

Fig. S1 relates to Fig. 1 and shows size standards and data supporting biochemical isolation of nodes. Fig. S2 relates to Fig. 3 and shows additional data supporting Wee1 localization bursts to Cdr2 nodes. Fig. S3 provides additional quantification of Cdr2 and Wee1 localization in *pom1Δ* mutant cells. Videos are TIRF microscopy videos of Wee1-mNeonGreen bursts (Video 1), Cdr2-mNeonGreen nodes (Video 2), and Cdr1-mNeonGreen nodes (Video 3). Table S1 lists yeast strains used in this study.

Acknowledgments

We thank members of the Moseley laboratory for comments on the manuscript as well as B. Wickner and C. Barlowe at Dartmouth for sharing equipment. We thank members of the A. Gladfelter laboratory and A. Lavanway for assistance with microscopy; A. Orr for assistance with ultracentrifugation; and J.-Q. Wu, T. Pollard, and D. Kellogg for sharing reagents and strains.

This work was supported by grants from the National Institutes of Health (R01 GM099774) and the American Cancer Society (RSG-15-140-01-CCG) to J.B. Moseley, a shared instrumentation grant from the National Institutes of Health (1S10OD018046),

a National Institutes of Health training grant (T32GM008704) to C.A.H. Allard, and the Dartmouth College Academic Summer Undergraduate Research Experience program for supporting U. Medoh.

The authors declare no competing financial interests.

Author contributions: J.B. Moseley and C.A.H. Allard conceived of the study; C.A.H. Allard, H.E. Opalko, U. Medoh, and K.-W. Liu performed experiments; all authors analyzed the data; J.B. Moseley and C.A.H. Allard wrote the manuscript.

Submitted: 29 September 2017
Revised: 7 December 2017
Accepted: 21 February 2018

References

Akamatsu, M., J. Berro, K.-M. Pu, I.R. Tebbs, and T.D. Pollard. 2014. Cytokinetic nodes in fission yeast arise from two distinct types of nodes that merge during interphase. *J. Cell Biol.* 204:977–988. https://doi.org/10.1083/jcb.201307174

Akamatsu, M., Y. Lin, J. Bewersdorf, and T.D. Pollard. 2017. Analysis of interphase node proteins in fission yeast by quantitative and super resolution fluorescence microscopy. *Mol. Biol. Cell.* 28:3203–3214. https://doi.org/10.1091/mbc.E16-07-0522

Aligue, R., L. Wu, and P. Russell. 1997. Regulation of Schizosaccharomyces pombe Wee1 tyrosine kinase. *J. Biol. Chem.* 272:13320–13325. https://doi.org/10.1074/jbc.272.20.13320

Bähler, J., J.Q. Wu, M.S. Longtine, N.G. Shah, A. McKenzie III, A.B. Steever, A. Wach, P. Philippsen, and J.R. Pringle. 1998. Heterologous modules for efficient and versatile PCR-based gene targeting in Schizosaccharomyces pombe. *Yeast.* 14:943–951. https://doi.org/10.1002/(SICI)1097-0061(199807)14:10%3C943::AID-YEA292%3E3.0.CO;2-Y

Bhatia, P., O. Hachet, M. Hersch, S.A. Rincon, M. Berthelot-Grosjean, S. Dalessi, L. Basterra, S. Bergmann, A. Paoletti, and S.G. Martin. 2014. Distinct levels in Pom1 gradients limit Cdr2 activity and localization to time and position division. *Cell Cycle.* 13:538–552. https://doi.org/10.4161/cc.27411

Breeding, C.S., J. Hudson, M.K. Balasubramanian, S.M. Hemmingsen, P.G. Young, and K.L. Gould. 1998. The cdr2(+) gene encodes a regulator of G2/M progression and cytokinesis in Schizosaccharomyces pombe. *Mol. Biol. Cell.* 9:3399–3415. https://doi.org/10.1091/mbc.9.12.3399

Coleman, T.R., Z. Tang, and W.G. Dunphy. 1993. Negative regulation of the wee1 protein kinase by direct action of the nim1/cdr1 mitotic inducer. *Cell.* 72:919–929. https://doi.org/10.1016/0092-8674(93)90580-J

Deng, L., and J.B. Moseley. 2013. Compartmentalized nodes control mitotic entry signaling in fission yeast. *Mol. Biol. Cell.* 24:1872–1881. https://doi.org/10.1091/mbc.E13-02-0104

Deng, L., S. Baldissard, A.N. Kettenbach, S.A. Gerber, and J.B. Moseley. 2014. Dueling kinases regulate cell size at division through the SAD kinase Cdr2. *Curr. Biol.* 24:428–433. https://doi.org/10.1016/j.cub.2014.01.009

Dolznig, H., F. Grebien, T. Sauer, H. Beug, and E.W. Müllner. 2004. Evidence for a size-sensing mechanism in animal cells. *Nat. Cell Biol.* 6:899–905. https://doi.org/10.1038/ncb1166

Fantes, P., and P. Nurse. 1977. Control of cell size at division in fission yeast by a growth-modulated size control over nuclear division. *Exp. Cell Res.* 107:377–386. https://doi.org/10.1016/0014-4827(77)90359-7

Feilotter, H., P. Nurse, and P.G. Young. 1991. Genetic and molecular analysis of cdr1/nim1 in Schizosaccharomyces pombe. *Genetics.* 127:309–318.

Gautier, J., M.J. Solomon, R.N. Booher, J.F. Bazan, and M.W. Kirschner. 1991. cdc25 is a specific tyrosine phosphatase that directly activates p34cdc2. *Cell.* 67:197–211. https://doi.org/10.1016/0092-8674(91)90583-K

Ginzberg, M.B., R. Kafri, and M. Kirschner. 2015. On being the right (cell) size. *Science.* 348:1245075. https://doi.org/10.1126/science.1245075

Gould, K.L., and P. Nurse. 1989. Tyrosine phosphorylation of the fission yeast cdc2+ protein kinase regulates entry into mitosis. *Nature.* 342:39–45. https://doi.org/10.1038/342039a0

Guzmán-Vendrell, M., S.A. Rincon, F. Dingli, D. Loew, and A. Paoletti. 2015. Molecular control of the Wee1 regulatory pathway by the SAD kinase Cdr2. *J. Cell Sci.* 128:2842–2853. https://doi.org/10.1242/jcs.173146

Hachet, O., M. Berthelot-Grosjean, K. Kokkoris, V. Vincenzetti, J. Moosbrugger, and S.G. Martin. 2011. A phosphorylation cycle shapes gradients of the DYRK family kinase Pom1 at the plasma membrane. *Cell.* 145:1116–1128. https://doi.org/10.1016/j.cell.2011.05.014

Harashima, H., N. Dissmeyer, and A. Schnittger. 2013. Cell cycle control across the eukaryotic kingdom. *Trends Cell Biol.* 23:345–356. https://doi.org/10.1016/j.tcb.2013.03.002

Kanoh, J., and P. Russell. 1998. The protein kinase Cdr2, related to Nim1/Cdr1 mitotic inducer, regulates the onset of mitosis in fission yeast. *Mol. Biol. Cell.* 9:3321–3334. https://doi.org/10.1091/mbc.9.12.3321

Keifenheim, D., X.-M. Sun, E. D'Souza, M.J. Ohira, M. Magner, M.B. Mayhew, S. Marguerat, and N. Rhind. 2017. Size-Dependent Expression of the Mitotic Activator Cdc25 Suggests a Mechanism of Size Control in Fission Yeast. *Curr. Biol.* 27:1491–1497. https://doi.org/10.1016/j.cub.2017.04.016

Kelkar, M., and S.G. Martin. 2015. PKA antagonizes CLASP-dependent microtubule stabilization to re-localize Pom1 and buffer cell size upon glucose limitation. *Nat. Commun.* 6:8445. https://doi.org/10.1038/ncomms9445

Kettenbach, A.N., L. Deng, Y. Wu, S. Baldissard, M.E. Adamo, S.A. Gerber, and J.B. Moseley. 2015. Quantitative phosphoproteomics reveals pathways for coordination of cell growth and division by the conserved fission yeast kinase pom1. *Mol. Cell. Proteomics.* 14:1275–1287. https://doi.org/10.1074/mcp.M114.045245

Kumagai, A., and W.G. Dunphy. 1991. The cdc25 protein controls tyrosine dephosphorylation of the cdc2 protein in a cell-free system. *Cell.* 64:903–914. https://doi.org/10.1016/0092-8674(91)90315-P

Lucena, R., M. Alcaide-Gavilán, S.D. Anastasia, and D.R. Kellogg. 2017. Wee1 and Cdc25 are controlled by conserved PP2A-dependent mechanisms in fission yeast. *Cell Cycle.* 16:428–435. https://doi.org/10.1080/15384101.2017.1281476

Martin, S.G., and M. Berthelot-Grosjean. 2009. Polar gradients of the DYRK-family kinase Pom1 couple cell length with the cell cycle. *Nature.* 459:852–856. https://doi.org/10.1038/nature08054

Masuda, H., C.S. Fong, C. Ohtsuki, T. Haraguchi, and Y. Hiraoka. 2011. Spatiotemporal regulations of Wee1 at the G2/M transition. *Mol. Biol. Cell.* 22:555–569. https://doi.org/10.1091/mbc.E10-07-0644

Moravcevic, K., J.M. Mendrola, K.R. Schmitz, Y.-H. Wang, D. Slochower, P.A. Janmey, and M.A. Lemmon. 2010. Kinase associated-1 domains drive MARK/PAR1 kinases to membrane targets by binding acidic phospholipids. *Cell.* 143:966–977. https://doi.org/10.1016/j.cell.2010.11.028

Moreno, S., J. Hayles, and P. Nurse. 1989. Regulation of p34cdc2 protein kinase during mitosis. *Cell.* 58:361–372. https://doi.org/10.1016/0092-8674(89)90850-7

Moreno, S., P. Nurse, and P. Russell. 1990. Regulation of mitosis by cyclic accumulation of p80cdc25 mitotic inducer in fission yeast. *Nature.* 344:549–552. https://doi.org/10.1038/344549a0

Moreno, S., A. Klar, and P. Nurse. 1991. Molecular genetic analysis of fission yeast Schizosaccharomyces pombe. *Methods Enzymol.* 194:795–823. https://doi.org/10.1016/0076-6879(91)94059-L

Morrell, J.L., C.B. Nichols, and K.L. Gould. 2004. The GIN4 family kinase, Cdr2p, acts independently of septins in fission yeast. *J. Cell Sci.* 117:5293–5302. https://doi.org/10.1242/jcs.01409

Moseley, J.B., A. Mayeux, A. Paoletti, and P. Nurse. 2009. A spatial gradient coordinates cell size and mitotic entry in fission yeast. *Nature.* 459:857–860. https://doi.org/10.1038/nature08074

Pan, K.Z., T.E. Saunders, I. Flor-Parra, M. Howard, and F. Chang. 2014. Cortical regulation of cell size by a sizer cdr2p. *eLife.* 3:e02040. https://doi.org/10.7554/eLife.02040

Parker, L.L., S.A. Walter, P.G. Young, and H. Piwnica-Worms. 1993. Phosphorylation and inactivation of the mitotic inhibitor Wee1 by the nim1/cdr1 kinase. *Nature.* 363:736–738. https://doi.org/10.1038/363736a0

Rincon, S.A., P. Bhatia, C. Bicho, M. Guzman-Vendrell, V. Fraisier, W.E. Borek, F. de L. Alves, F. Dingli, D. Loew, J. Rappsilber, et al. 2014. Pom1 regulates the assembly of Cdr2-Mid1 cortical nodes for robust spatial control of cytokinesis. *J. Cell Biol.* 206:61–77. https://doi.org/10.1083/jcb.201311097

Russell, P., and P. Nurse. 1986. cdc25+ functions as an inducer in the mitotic control of fission yeast. *Cell.* 45:145–153. https://doi.org/10.1016/0092-8674(86)90546-5

Russell, P., and P. Nurse. 1987. Negative regulation of mitosis by wee1+, a gene encoding a protein kinase homolog. *Cell.* 49:559–567. https://doi.org/10.1016/0092-8674(87)90458-2

Saunders, T.E., K.Z. Pan, A. Angel, Y. Guan, J.V. Shah, M. Howard, and F. Chang. 2012. Noise reduction in the intracellular pom1p gradient by a dynamic clustering mechanism. *Dev. Cell.* 22:558–572. https://doi.org/10.1016/j.devcel.2012.01.001

Sbalzarini, I.F., and P. Koumoutsakos. 2005. Feature point tracking and trajectory analysis for video imaging in cell biology. *J. Struct. Biol.* 151:182–195. https://doi.org/10.1016/j.jsb.2005.06.002

Simanis, V., and P. Nurse. 1986. The cell cycle control gene cdc2+ of fission yeast encodes a protein kinase potentially regulated by phosphorylation. *Cell.* 45:261–268. https://doi.org/10.1016/0092-8674(86)90390-9

Strausfeld, U., J.C. Labbé, D. Fesquet, J.C. Cavadore, A. Picard, K. Sadhu, P. Russell, and M. Dorée. 1991. Dephosphorylation and activation of a p34cdc2/cyclin B complex in vitro by human CDC25 protein. *Nature.* 351:242–245. https://doi.org/10.1038/351242a0

Wood, E., and P. Nurse. 2013. Pom1 and cell size homeostasis in fission yeast. *Cell Cycle.* 12:3417–3425. https://doi.org/10.4161/cc.26462

Wu, J.-Q., and T.D. Pollard. 2005. Counting cytokinesis proteins globally and locally in fission yeast. *Science.* 310:310–314. https://doi.org/10.1126/science.1113230

Wu, L., and P. Russell. 1993. Nim1 kinase promotes mitosis by inactivating Wee1 tyrosine kinase. *Nature.* 363:738–741. https://doi.org/10.1038/363738a0

Wu, L., K. Shiozaki, R. Aligue, and P. Russell. 1996. Spatial organization of the Nim1-Wee1-Cdc2 mitotic control network in Schizosaccharomyces pombe. *Mol. Biol. Cell.* 7:1749–1758. https://doi.org/10.1091/mbc.7.11.1749

Young, P.G., and P.A. Fantes. 1987. Schizosaccharomyces pombe mutants affected in their division response to starvation. *J. Cell Sci.* 88:295–304.